American Mineralogist, Volume 81, pages 685–695, 1996

Graphical analysis of pigeonite-augite liquidus equilibria

J. LONGHI[1] AND C.M. BERTKA[2]

[1]Lamont-Doherty Earth Observatory, Palisades, New York 10964, U.S.A.
[2]Geophysical Laboratory and the Center for High Pressure Research, 5251 Broad Branch Road NW, Washington, DC 20015, U.S.A.

ABSTRACT

A combination of experimental and topological constraints indicates that critical equilibria play an important role in determining the pyroxene-liquid phase relations along the $Mg_2Si_2O_6$-$CaMgSi_2O_6$ (enstatite-diopside) join and in natural lherzolites. Topological constraints do not permit the three-pyroxene equilibrium, orthopyroxene + diopside = pigeonite, to intersect either of the two melting equilibria, pigeonite + diopside = liquid or pigeonite = orthopyroxene + liquid in the enstatite-diopside join. Thus, with increasing pressure, pigeonite cannot abruptly replace diopside on the solidus of simplified lherzolites in this join. A supercritical low-Ca clinopyroxene, however, can replace diopside with increasing pressure along the solidus in the following manner: As the temperature of the solidus sweeps up the orthopyroxene + diopside two-phase field, the solidus crosses that region of the two-phase field where the diopside-rich limb of the two-phase field is inflected sharply toward enstatite by the proximal top of the metastable pigeonite + diopside solvus; once the solidus is at a higher temperature than the top of the metastable solvus, the diopside coexisting with orthopyroxene becomes supercritical and its Ca content drops rapidly but continuously.

In the natural system and its synthetic analogs pigeonite may replace augite on the lherzolite solidus (orthopyroxene + augite + olivine + plagioclase + liquid) at constant pressure and decreasing Mg′ [MgO/(MgO + FeO)] as the solidus liquid, which becomes less aluminous, intersects the liquid coexisting with orthopyroxene + pigeonite + augite, which becomes more aluminous with decreasing Mg′. However, with Mg′ and the normative feldspar composition of the liquid nearly constant, the solidus liquid becomes sufficiently more aluminous with increasing pressure to prevent the three-pyroxene equilibrium from overtaking and intersecting the lherzolite solidus. Thus, in the natural system as in the enstatite-diopside join, pigeonite does not replace augite abruptly. Rather, the replacement of augite by low-Ca clinopyroxene with increasing pressure is relatively gradual and is influenced by the presence of a pseudoternary pigeonite + augite solvus. Experimental evidence suggests that the top of the solvus emerges from the local solidus at 13–15 kbar and forms a critical end point to the pigeonite + augite + olivine liquidus boundary. The emergence of the critical end point distorts both the remaining liquidus boundaries and the clinopyroxene solid-solution surface, such that the CaO content of the clinopyroxene (now supercritical) coexisting with orthopyroxene decreases more rapidly with further increases in pressure. The critical end point migrates to the orthopyroxene-wollastonite join in just a few kilobars and completely eliminates the pigeonite + augite + olivine liquidus boundary curve by ~18 kbar.

INTRODUCTION

Pyroxene liquidus equilibria play an important role in basalt petrogenesis. Recently, Bertka and Holloway (1993) made an especially interesting observation of pyroxene equilibria relevant to basalt petrogenesis. They observed that with increasing pressure low-Ca or "pigeonitic" clinopyroxene (Cpx) replaces high-Ca clinopyroxene on the anhydrous solidus of DW, a model martian mantle composition (Dreibus and Wänke 1985), equivalent to an Fe-rich lherzolite (olivine + orthopyroxene + clinopyroxene ± plagioclase, spinel, garnet). They also cited several examples from the literature (e.g., Takahashi 1986) of similar low-Ca clinopyroxenes in high-pressure experiments on more magnesian terrestrial peridotites. Subsequently, Longhi (1995) showed that low-Ca clinopyroxenes (6–7 wt% CaO) coexist with olivine (Ol), orthopyroxene (Opx), garnet (Gar), and liquid (liq) in the range of 28–30 kbar for a series of lunar (low-alkali) compositions with Mg′ [molar MgO/(MgO + FeO)] spanning the range of martian and terrestrial values.

In addition to being vitally important to anyone at-

0003–004X/96/0506–0685$05.00

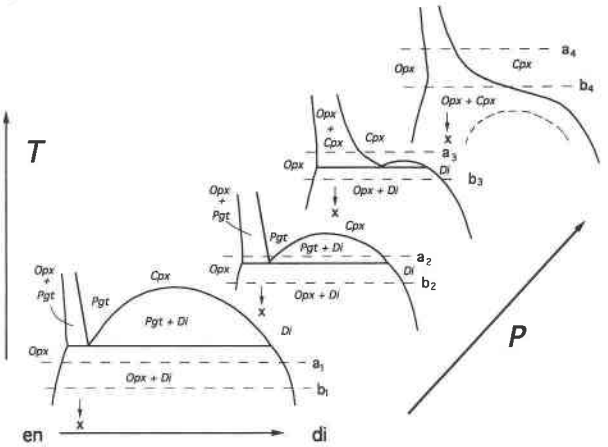

FIGURE 1. Schematic temperature-pressure-composition relations for the En-Di join from 1 atm to ~30 kbar. Equilibria involving protoenstatite, Fo, and liquid are omitted. Abbreviations of phase names are explained in the text. Dashed lines a_1-a_2-a_3-a_4 and b_1-b_2-b_3-b_4 are hypothetical solidus surfaces of two natural basaltic liquids. The a solidus intersects the three-pyroxene equilibrium Opx + Di = Pgt. The critical equilibrium, Pgt + Di = Cpx, eliminates the three-pyroxene equilibrium before the b solidus can intersect it. The "x" is a model peridotite composition.

tempting to model melting equilibria, the replacement of high-Ca clinopyroxene by low-Ca clinopyroxene on the lherzolite solidus with increasing pressure has important geochemical implications. Because of the well-established positive correlation of REE partition coefficients with the Ca content of clinopyroxenes (McKay et al. 1986), the partition coefficients of Cpx at high pressures are probably much lower (~D^{Opx}) than at low pressures, where most of the partition coefficients have been measured. Thus, many calculations of percent melting and relative proportions of Opx and Cpx in basalt source regions may need to be reexamined.

Despite several observations of low-Ca clinopyroxene on the lherzolite solidus at high pressure, the actual transformation of high- to low-Ca Cpx has not yet been tightly constrained by experiments. Thus, judgments on the nature of the transformation depend upon extrapolations of experimental data and topological arguments. Bertka and Holloway (1993) discussed two mechanisms: One involves an intersection of the solidus with the equilibrium between orthopyroxene and two clinopyroxenes and thus produces a relatively abrupt change in clinopyroxene composition; the other involves two-clinopyroxene critical equilibria and produces a more gradual change. Bertka and Holloway (1993) argued for the former mechanism in the case of the martian (DW) composition but left the case of terrestrial lherzolite unspecified. However, Longhi (1995) argued that experimental data were consistent with critical phenomena playing the decisive role in all cases, including DW. We now present a more thorough examination of the experimental data and topological constraints relevant to the change in composition of the solidus clinopyroxene.

In the following discussion we distinguish where possible between subcritical and supercritical clinopyroxenes. The terms "pigeonite" (Pgt) and "augite" (Aug) are reserved for low-Ca and high-Ca clinopyroxene, respectively, that share a common free-energy surface with an intervening unstable region; hence, pigeonite and augite may coexist on opposite limbs of a solvus. Diopside (Di) is the Fe-free equivalent of augite. "Clinopyroxene" is necessarily ambiguous, but in equations or phase diagrams its abbreviated form, Cpx, refers to a clinopyroxene with no unstable region on its free-energy surface and, hence, no miscibility gap. So Cpx is the phase designation at temperatures above the critical or consolute point of the pigeonite + augite solvus.

THE JOIN $Mg_2Si_2O_6$-$CaMgSi_2O_6$

Phase equilibria in the enstatite-diopside (En-Di) join provide a basis for understanding the possible equilibria involving pyroxene and liquid. Unfortunately, because of multiple polymorphism, displacive transformations, and incongruent melting of the low-Ca pyroxenes at low-pressure, phase diagrams of the En-Di join (e.g., Longhi and Boudreau 1980; Carlson 1988) are quite complicated, so equilibria involving protoenstatite and incongruent melting, which are restricted to low pressures, are omitted, and only the equilibria (mostly metastable) involving orthopyroxene and the two clinopyroxenes Pgt and Di are depicted schematically in Figure 1. At low pressure a univariant equilibrium (Opx + Di = Pgt) separates a low-temperature assemblage of Opx + Di from possible high-temperature assemblages of Opx + Pgt, Pgt, and Pgt + Di. At still higher temperatures the Pgt + Di solvus terminates at a consolute or critical point. At higher pressure the experimental work of Lindsley and Dixon (1976) and Schweitzer (1982) showed that the temperature of the three-pyroxene equilibrium increases sufficiently to intersect the critical point at $T < 1500$ °C and $P < 20$ kbar. At this intersection the distinction between Pgt and Di disappears, the entire Pgt + Di solvus becomes metastable, and the three-pyroxene equilibrium is thus eliminated. Consequently, at higher pressure there is only a two-phase field between orthopyroxene and a single clinopyroxene phase. In addition, the metastable solvus distorts the Opx + Cpx field such that at temperatures near the metastable critical point the Cpx-limb of the Opx + Cpx field is deflected toward Di-poor compositions. Thus, at temperatures higher than the metastable critical point, clinopyroxene coexisting with orthopyroxene is relatively CaO poor. The works of Huebner and Turnock (1980) and Lindsley and Anderson (1983) showed that the low-pressure topology illustrated in Figure 1 extends to pyroxenes with Mg′ ≈ 0.3. Sparse work at higher pressures has shown a small, but distinct two-phase field between Pgt and Aug (Fe-bearing Di) with Mg′ in the range of 0.4–0.1 at 15 kbar (Lindsley 1983).

The two possible mechanisms for obtaining low-Ca or pigeonitic clinopyroxene coexisting with orthopyroxene

can be understood by considering two hypothetical solidi with respect to both the pyroxene equilibria and a model lherzolite composition x shown in Figure 1 (here we are deliberately mixing binary and multicomponent equilibria for the sake of illustration). In natural systems variations of additional components may be expected to affect solidus temperatures much more than equilibria involving only pyroxenes, so the positions of the pyroxene equilibria at each pressure are shown to be the same for the two solidi as a convenient approximation. The solidus with the higher temperature (a_1, a_2, a_3, a_4) intersects at Opx + Di = Pgt equilibrium between the first two isobaric sections, and thus a low-Ca Pgt abruptly replaces a high-Ca Di on the solidus. This sequence is consistent with the observation by Bertka and Holloway (1993) of augite (16 wt% CaO) on the DW solidus at 5 kbar replaced by "pigeonite" (9 wt% CaO) at 15 kbar. The other solidus (b_1, b_2, b_3, b_4) does not intersect the three-pyroxene equilibrium but instead rolls over the inflected limb of the Opx + Cpx two-phase field, such that at $P > 20$ kbar Opx coexists with a low-Ca supercritical Cpx.

Although the analysis presented in Figure 1 is a useful introduction to some of the possible configurations in the natural system, projections of multicomponent melting equilibria onto end-member two-component planes are incapable of portraying all the complexities of the natural system. However, simple systems do provide an important framework on which to build a clear understanding of complex phase equilibria. So before proceeding with an analysis of the natural system, we first consider the pressure-temperature topology of solidus-solvus interactions in the En-Di join.

The example of the two solidi translates into two possible topologies for univariant equilibria involving pyroxenes and liquid along the En-Di join. One involves intersection of the three-pyroxene equilibrium with the solidus, the other involves intersection of the three-pyroxene equilibrium with the Pgt-Di critical curve. As a starting point consider Figure 2, another simplified phase diagram of the En-Di join at 1 bar. Equilibria involving forsterite (Fo) and protoenstatite are still omitted, but now melting equilibria (mostly metastable) are included. In contrast to the low-pressure section in Figure 1, the critical point is now metastable with respect to liquid. Other additional features include incongruent melting of Pgt to Opx + liq, a eutectic between Di and Pgt, a stable maximum on the Di liquidus near the $CaMgSi_2O_6$ composition, and a minimum (not shown) on the Di liquidus that is metastable with respect to the Pgt + Di solvus. Despite being metastable with respect to protoenstatite- or Fo-bearing assemblages, the various univariant equilibria depicted in Figure 2 are well constrained in terms of temperature. The temperatures of the two melting equilibria can be obtained by extrapolation of the Opx + Pgt and Pgt + Di liquidus boundaries to the En-Di join in the 1 atm liquidus diagram for Mg_2SiO_4-$CaMgSi_2O_6$-SiO_2 (Longhi and Boudreau 1980); and the 1 bar temperatures of the Opx + Di = Pgt equilibrium and the

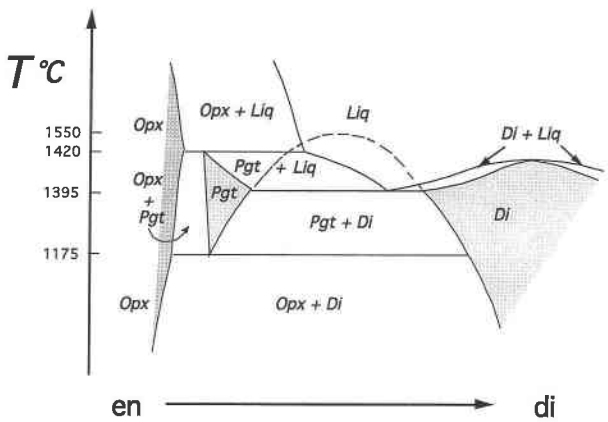

Figure 2. Schematic temperature-composition relations for the En-Di join at 1 atm, excluding equilibria that involve protoenstatite and Fo but including liquidus equilibria (some metastable). Dashed curve is the metastable portion of the Pgt-Di solvus. Temperatures are extrapolated from Figure 1 of Longhi and Boudreau (1980) and from Figure 2 of Carlson and Lindsley (1988), as explained in the text.

critical point can both be obtained by extrapolation of their respective curves in Figure 2 of Carlson and Lindsley (1988). The two melting equilibria, Pgt + Di = liq and Pgt = Opx + liq, presumably have positive slopes in P-T space; Carlson and Lindsley (1988) and Gasparik (1990) calculated a positive slope for Opx + Di = Pgt and a slightly negative slope for the critical curve; and melting experiments have yielded an initial slope of 15 °C/kbar for the Di liquidus that decreases to 10 °C/kbar between 10 and 30 kbar (Boyd and England 1963).

These constraints yield two basic P-T arrays of the univariant equilibria as shown in Figure 3. Although some pressures and temperatures are known, the diagrams are not drawn to scale for the sake of clarity. Figure 2 serves as the 1 atm temperature-composition section for both Figures 3a and 3b. Several additional isobaric sections are drawn to illustrate the compositional relations at higher pressures. The shallow slope of the liquidus to the left of the maximum (M) near Di indicates that the minimum (m) is only marginally metastable. This feature plus the steep T-P slope of the Di liquidus suggest that the first major change in topology in both cases probably occurs when the metastable minimum on the En-Di liquidus emerges from the Pgt + Di field and changes the Pgt + Di eutectic to a peritectic where the equilibrium is Di = Pgt + liq. In the P-T plane the emergence of the minimum is an invariant point (m′) where the univariant equilibrium Di_m or Cpx_m = liq (light solid line) is the tangent to the Pgt-Di-liq curve. Although other topologies are possible, liquidus data at 20 kbar are consistent with the presence of a minimum at least on the liquidus of the En-Di join (Kushiro 1969, Fig. 3; Lindsley 1980, Fig. 8c). Both the minimum and maximum are univariant equilibria that may extend to much higher pressures

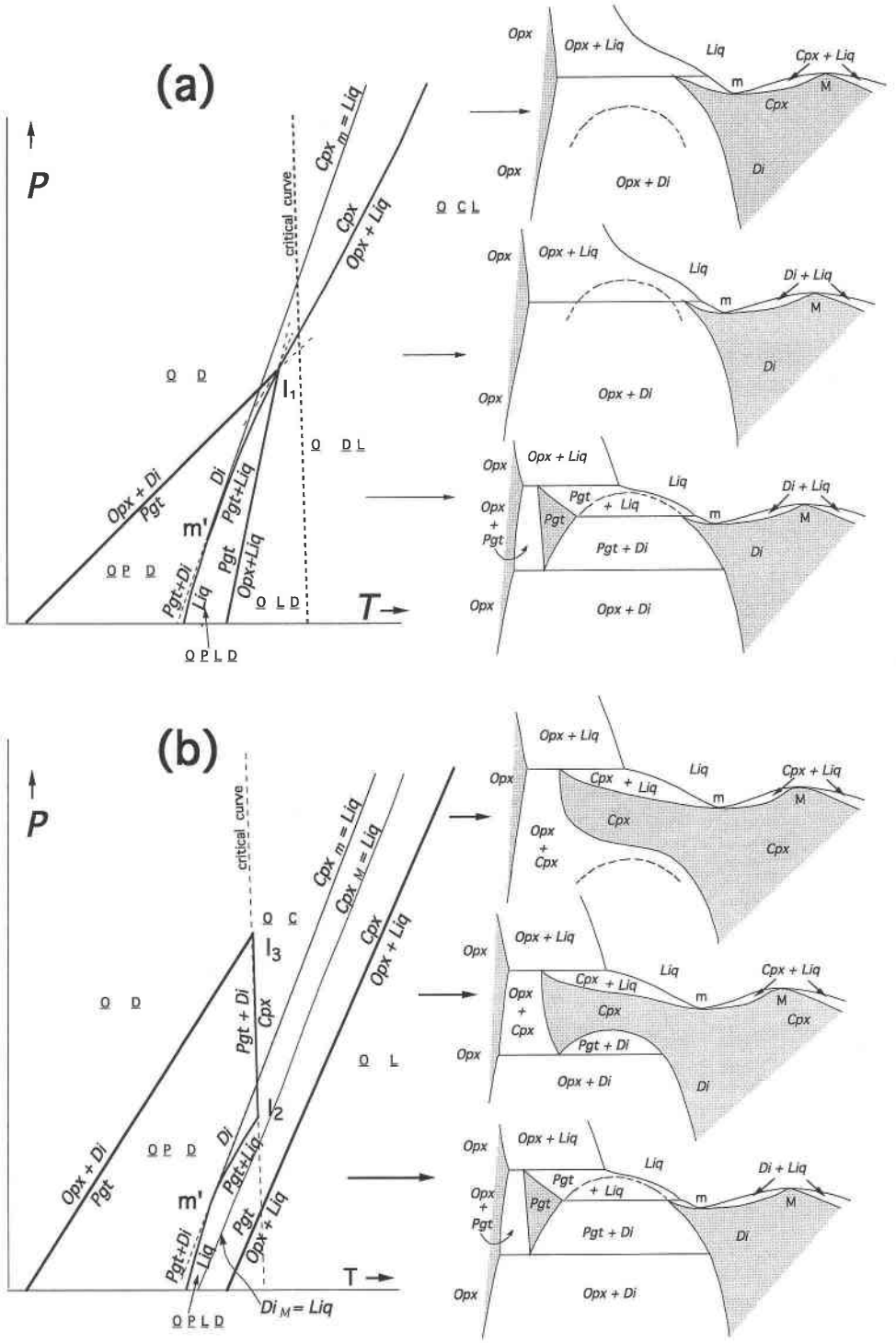

FIGURE 3. Two possible topologies of temperature-pressure-composition equilibria for the En-Di join, excluding equilibria that involve protoenstatite and Fo. Large arrows show the appropriate pressure for the isobaric temperature-composition sections to the right. Figure 2 shows the topology of the lowest pressure section of both **a** and **b**. (**a**) Critical curve (Pgt + Di = Cpx) is metastable throughout *P-T* range, and the solidus curves and three-pyroxene equilibrium intersect at I_1. Invariant point m′ is where Di and liq with the same composition coexist with Pgt. (**b**) Portions of critical curve are stable and intersect both the two-clinopyroxene solidus (I_2) and the three-pyroxene equilibrium (I_3). The univariant curve Cpx_M = liq, which represents the maximum on the Di liquidus surface and which should lie a few degrees above and subparallel to the Cpx_m = liq curve in the *P-T* sections, is omitted from the *P-T* section in **a**. Abbreviations as in text, except for phase labels in divariant fields of *P-T* section: O = Opx, P = Pgt, D = Di, L = liq, C = Cpx.

($\geq$100 kbar) before intersecting other equilibria (Gasparik 1994). The *P-T* curve of the maximum (Di_M or Cpx_M = liq) lies a few degrees above that of the minimum in both constructions but is not shown in Figure 3a to avoid clutter. In the case of Figure 3a, all three-phase equilibria are constrained to meet at a single invariant point (I_1) where the two solidi overtake the three-pyroxene curve. This invariant point is topologically possible at positive pressures (with or without the emergence of the liquidus minimum) only if the critical curve is everywhere metastable and only if the *P-T* slope of the three-pyroxene curve is shallower than those of the two melting curves. In Figure 3b the metastable critical point pulls out of the Pgt + liq field and terminates the Di = Pgt + liq univariant curve at the invariant point (I_2) where the critical Cpx coexists with liq. At higher pressure, but lower temperature, the Opx + Di = Pgt univariant curve overtakes the critical point and is eliminated at the invariant point (I_3) where the critical clinopyroxene coexists with orthopyroxene. At still higher pressures the critical curve becomes metastable again as the top of the solvus pulls down into the Opx + Di field. The abrupt termination of univariant equilibria without metastable extensions means that if the clinopyroxene critical curve becomes stable, the invariant point (I_1) depicted in Figure 3a becomes impossible, even metastably.

An apparent conflict exists among the available experimental data bearing on the correct topology. Kushiro (1969; Fig. 3) showed a wide separation of the Pgt + Di solvus and a near conjunction of the three-pyroxene equilibrium and the two solidus equilibria at 20 kbar and ~1650 °C, thus favoring the topology in Figure 3a. On the other hand, experimental work of Lindsley and coworkers cited above demonstrated that at least the higher pressure invariant point (I_3) in Figure 3b (critical Cpx + Opx) is stable between 15 and 20 kbar. Carlson and Lindsley (1988) extracted thermodynamic parameters from reversed equilibria in this system and calculated the temperature and pressure of this invariant point (I_3) to be approximately 1450 °C and 18 kbar. Gasparik (1990) obtained similar results. If these calculations are accurate, they indicate that the presence of a Pgt + Di solvus at 1650 °C and 20 kbar in Kushiro's (1969) diagram of En-Di is an artifact of metastable solid solutions. Given the high quality of the data on which Carlson and Lindsley (1988) based their calculations and the possibility of metastable solid solutions in Kushiro's relatively short subsolidus experiments (15 min to 1 h at 1600 °C), it is highly probable that the subsolidus portions of Kushiro's (1969) diagram are incorrect and that invariant point I_2 in Figure 3b is stable at 1450 °C and 18 kbar. Furthermore, if I_3 is stable, then simple geometry requires that the lower pressure invariant point, I_2, involving the critical Cpx and coexisting liquid, be stable also [Carlson and Lindsley (1988) calculated its pressure at ~5 kbar]. Therefore, Figure 3b is the correct topology, and the solidus does not overtake the three-pyroxene curve in this system at least. Rather, Di coexisting with Opx and liq progressively becomes lower in CaO with increasing pressure and is eventually replaced at I_2 by a supercritical clinopyroxene.

Other simple systems

Hydrothermal experiments by Lindsley (1981) indicated a high-pressure topology for pyroxenes in the $Fe_2Si_2O_6$(Fo)-$CaFeSi_2O_6$(Hd) join that is very similar to that shown in Figure 1, except that the temperatures are much lower: Between 15 and 20 kbar the Opx + Hd = Pgt equilibrium intersects the critical point on the two-clinopyroxene solvus ($T \approx 875$ °C), leaving only orthopyroxene and supercritical clinopyroxene at higher temperature and pressure. Thus, the general topology in Figure 3b probably holds for constant Mg′ sections through the pyroxene quadrilateral. However, even though phase relations on the end-member joins suggest that the pressure at which the three-pyroxene curve disappears remains nearly constant, the thermodynamic model of Sack and Ghiorso (1994) predicts a ballooning of the stability of the three-pyroxene assemblage from 20 to 40 kbar at intermediate to low Mg′ (0.7–0.05) in Pgt. These values of Mg′ are much lower than those of the pyroxenes discussed below.

Univariant equilibria in the CaO-MgO-Al_2O_3-SiO_2 (CMAS) system probably have a topology analogous to that in Figure 3b, but insufficient data on coexisting aluminous clinopyroxenes limit the type of constrained topological analysis that was possible in the case of En-Di. However, comparison of the compositions of Al-bearing Pgt and Di pairs from CMAS at 1 atm (Longhi 1987) with those of Al-free Pgt and Di pairs from the En-Di join (Carlson 1988) shows that in isothermal sections the Cpx solvus closes with the addition of the Tschermak component (Ca^{2+},Mg^{2+} + Si^{4+} = $2Al^{3+}$). Thus, the highest possible temperature on the Cpx solvus at any pressure is the critical point on the En-Di join, and, by extension, the highest possible pressure for coexisting Pgt and Di in CMAS is that of invariant point I_3 (18 kbar) in Figure 3b. These features have important implications for the natural system discussed below but are in conflict with the calculations of Herzberg and Gasparik (1991; Fig. 4), which showed the limit of the Pgt + Di field in CMAS to be near the model lherzolite solidus at approximately 22 kbar. These results imply either that the experimental bracketing of *P* and *T* for I_2 is in error or that the Cpx solvus widens with Al substitution. We prefer the interpretations that agree most closely with the experimental data and suspect that more data on aluminous Pgt + Di pairs at high pressure are needed to construct accurate thermodynamic models.

Some further inferences from experimental data are possible. For example, if we define the model lherzolite solidus as the coexistence of Ol, Opx, Cpx (super- or subcritical), an aluminous phase [plagioclase (Pl) → spinel → garnet with increasing pressure], and liquid, then the composition of the Cpx provides a clue about solvus-solidus interactions. In CMAS the data of Walter and Presnall (1994) show that Cpx on the lherzolite solidus remains relatively constant in composition and high in

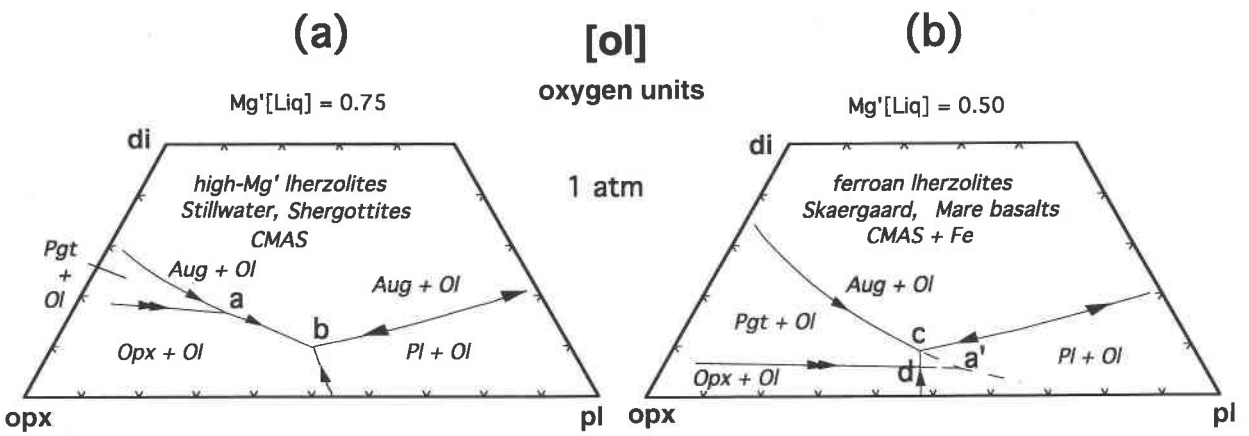

FIGURE 4. Examples of the two different topologies on the Ol liquidus surface at 1 atm. The surface is projected from the Ol component onto the lower half of the Opx-Wo-Pl component join. Liquidus boundaries are calculated for the values of Mg′ in the liquid as shown in the figure from the algorithms of Longhi (1991); the albite and orthoclase fractions of the normative feldspar, Nab and Nor, are the same in **a** and **b**, 0.40 and 0.02, respectively. Arrows indicate direction of decreasing temperature; double arrows indicate reaction boundaries. Some examples are given of rock types and localities where crystal assemblages imply the topology shown in the figure. The letters a, b, c, and d refer to pseudounivariant (isobaric pseudoinvariant) equilibria: a = Opx + Pgt + Aug + Ol + liq, b = Opx + Aug + Pl + Ol + liq, c = Pgt + Aug + Pl + Ol + liq, and d = Opx + Pgt + Pl + Ol + liq. The a′ is metastable a.

CaO (~19 wt%) from 1 atm to 11 kbar; at 20 kbar CaO in the Cpx has dropped to 16%; and at 30 kbar CaO has dropped to 13%. Data at 80 kbar (Herzberg and Gaparik 1991) show a further decrease to 9%. This slow decrease in CaO is inconsistent with an abrupt reaction in which Pgt replaces Di. However, the modest CaO concentration at 20 kbar is at least consistent with a supercritical Cpx. Analogous data in the Na_2O-CaO-MgO-Al_2O_3-SiO_2 system (Walter and Presnall 1994) show a similar decrease in CaO with pressure, although interpretation is complicated by high contents of the jadeite component. Arguments presented below suggest that the effect of critical phenomena on the composition of the Cpx at the lherzolite solidus should be more pronounced in Fe-bearing systems.

THE NATURAL SYSTEM

Although here, too, insufficient data hinder a constrained topological analysis, some additional inferences can be made from the shift of liquidus boundaries with pressure combined with constraints from the simple systems. Multicomponent equilibria are effectively portrayed by the projection method in which liquid compositions are projected from the composition of a ubiquitous saturating phase onto a convenient join, for which the liquidus relations in an analogous simple system are well known. The projection image can be sharpened further by restricting the compositions of the phases in a given frame. For example, Mg′ and normative feldspar composition may be held approximately constant (Longhi 1991).

Projecting from the Ol component is most useful for portraying pyroxene equilibria in basaltic systems. At 1 atm there are two general topologies of the Ol liquidus surface (Fig. 4) that are well constrained by experiments in both the CMAS and natural systems. The actual liquidus boundaries are drawn from the algorithms of Longhi (1991). Figure 4a shows the topology of the CMAS system and high Mg′ natural liquids (minus protoenstatite) in which Opx, Aug, and Pl coexist with Ol and liq, whereas Pgt does not coexist with Pl because it is restricted to Al-poor liquids. Figure 4b depicts the topology of liquids with intermediate Mg′ in which Pgt, Aug, and Pl coexist with Ol and liq, and Opx does not coexist with Aug. Figure 4a represents primitive Stillwater magmas, some magnesian tholeiites, and low-pressure melts of terrestrial peridotite; Figure 4b represents evolved tholeiites (Skaergaard), mare basalts, and eucrites. The important pseudounivariant equilibria, some of which have analogs in Figure 3, are labeled with letters. The label a is the three-pyroxene equilibrium (+ Ol + liq); b is the magnesian lherzolite solidus (Opx + Aug + Pl); c and d can be though of as possible solidi of lherzolites with intermediate Mg′. Lherzolites with relatively high wollastonite (Wo) contents (Pgt + Aug) begin melting at c, peridotites with low Wo contents (Opx + Pgt) begin melting at d, and those with intermediate Wo may begin melting between c and d because in these cases all the Wo component is accommodated in Pgt solid solution. It should be clear, however, that even though the solidi of certain assemblages can be narrowly defined, the solidus of the system covers a wide range of temperature, composition, and mineral assemblages.

Longhi and Pan (1988) demonstrated a continuous change on topology from that in Figure 4a to that in Figure 4b caused by the progressive decrease in Mg′ at 1 atm

and constant normative alkali feldspar component. As Mg′ decreases the Pgt liquidus field in Figure 4a expands with respect to that of Opx, forcing point a to migrate to the right. At the same time the Pl liquidus field expands with respect to the pyroxene fields, forcing point b to the left. When a and b meet, the topology in Figure 4b is generated and point a becomes metastable within the Pl + Ol liquidus field. Increasing the alkali content of the normative feldspar at constant Mg′ has relatively little effect on the size of the Pgt field but does expand the pyroxene liquidus fields relative to Pl, forcing point b to the right. Thus, it is possible to have two compositions with the same Mg′, one which is more alkaline and produces an assemblage of Opx + Aug (+ Ol + Pl + liq) and one which is less alkaline and produces a Pgt + Aug or Opx + Pgt (+ Ol + Pl + liq) assemblage. From the point of view of our analysis, however, the meeting of points a and b is also the intersection of the three-pyroxene equilibrium with the lherzolite solidus. Thus, if increasing pressure at constant composition can change the topology of the Ol liquidus surface from that in Figure 4a to that in Figure 4b, then Pgt may abruptly replace augite on the lherzolite solidus as proposed by Bertka and Holloway (1993) and illustrated in Figure 1. If not, then a solvus-solidus interaction is required to account for low-Ca clinopyroxene on the lherzolite solidus.

Unfortunately, the only fairly extensive mapping of high-pressure liquidus boundaries on the Ol surface in constant Mg′ sections has been done in the range of 28–30 kbar (Longhi 1995), where only one Cpx is stable. There are, however, extensive data on the composition of melts coexisting with lherzolite assemblages at modest pressures (≤20 kbar), which locally provide constraints on the topology of the liquidus boundaries. These liquidus boundaries may then be compared to those with similar Mg′ and normative feldspar composition at low pressure to observe pressure-induced shifts in liquidus boundaries at constant composition. Figure 5 presents representative examples from the literature of high-pressure liquids saturated with Ol, pyroxene, and an aluminous phase (spinel). The terrestrial and martian examples fix the lherzolite solidus for their respective compositions; the lunar datum fixes only the position of the Ol + Opx + Sp liquidus boundary and constrains the Ol + Cpx boundary to lie at some higher Wo content, which is estimated here from well-constrained positions of this boundary at both lower and higher pressure (e.g., Longhi 1995). Low-pressure liquidus boundaries for liquids with the same Mg′ and normative feldspar composition as the high-pressure examples were calculated from the algorithms of Longhi (1991). Examination of Figure 5 shows that in each case the pyroxene fields expand at the expense of the field of the aluminous phase (spinel in the range of 10–15 kbar), and, consequently, the Mg-rich lherzolite solidus (point b) moves away from the three-pyroxene curve (point a). The datum on the Mars composition (Bertka and Holloway 1994) shows the largest pressure shift. This shift is enhanced by the high value of

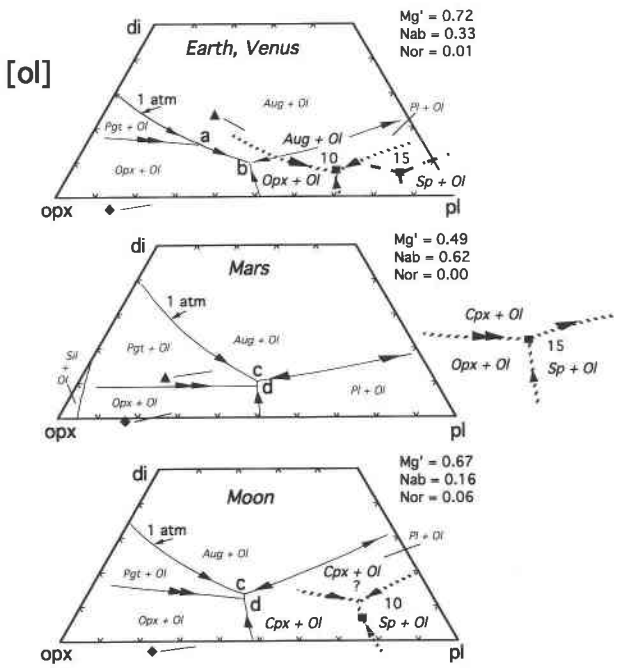

FIGURE 5. Comparison of the relative positions of 1 atm and high-pressure liquidus boundaries in a variety of magma types. Projections as in Figure 4. One atmosphere liquidus boundaries (light solid curves and light field labels) calculated from the algorithms of Longhi (1991), with Mg′, Nab, and Nor inputs taken from high-pressure liquid compositions. Nab values of 0.33, 0.62, and 0.16 correspond to approximately 2, 3, and 1 wt% Na_2O, respectively. High-pressure liquidus boundaries (heavy dashed curves and heavy field labels) drawn from experimental data: top, terrestrial lherzolite, Takahashi (1986) and Falloon and Green (1988); middle, model martian lherzolite, Bertka and Holloway (1994); bottom, model bulk Moon, Delano (1977). Bold numbers are pressure in kilobars. Squares = multisaturated liquids, triangles = Cpx, diamonds = Opx, Sp = spinel. Short lines near solid compositions are truncated tielines to coexisting liquid.

Nab, corresponding to a combination of high Al_2O_3 and Na_2O. Multisaturated 16 kbar liquids with similar compositional parameters reported by Kinzler and Grove (1992) project in similar positions. Also, the Mars datum shows the Opx + Ol liquidus field expanding with respect to the Ol + Pgt and Ol + Aug liquidus fields with increasing pressure. Longhi (1995) also noted this expansion at 30 kbar in lunar compositions with intermediate Mg′. In the case of the more magnesian terrestrial compositions in Figure 5, little change occurs in the relative position of the boundary between the fields of orthopyroxene and those of the clinopyroxenes. These observations imply that it is difficult for the three-pyroxene equilibrium (point a) to migrate to the right sufficiently with increasing pressure so as to overtake the lherzolite solidus (point b), although, geometrically, it is still possible for point a to migrate to the right if the Pgt + Aug (+ Ol) liquidus boundary shifts to greater Wo faster than the

Opx + Pgt (+ Ol) boundary. Thus, intersection of the two pseudounivariant equilibria, a and b, with increasing pressure and constant composition seems unlikely once they are stably separated. However, for compositions with the right combination of Mg′ and normative alkali feldspar (such as those shown in the martian and lunar panels in Fig. 5), point a is only marginally metastable at low pressure, and increasing pressure may force the three-pyroxene equilibrium to emerge from the Pl + Ol field. This emergence would change a solidus assemblage of Opx + Pgt + Ol + Pl (point d) or Pgt + Aug + Ol + Pl (point c) at low pressure to Opx + Aug + Ol + Pl (or Sp) at higher pressure. Elimination of Pgt in this way may account for the coexistence of Opx and Aug in the 5 kbar experiments of Bertka and Holloway (1993) on the DW composition despite the relatively low Mg′.

A CRITICAL END POINT

The previous discussions focused primarily on proving that intersection of the three-pyroxene equilibrium does not produce a low-Ca Cpx on the lherzolite solidus with increasing pressure. The low-Ca Cpx observed by several investigators must, therefore, be related to Cpx critical phenomena. The only hard constraints are that the distinction between Pgt and Aug in the En-Di join disappears at about 18 kbar, and that at some lower pressure ($\geq$5 kbar) the critical Cpx coexists with liquid. The various arguments presented above imply that similar constraints apply to the natural system as well. Thus, in addition to low-Ca Cpx appearing on the lherzolite solidus, the Pgt + Aug (+ Ol) liquidus boundary curves depicted in Figures 4 and 5 must disappear entirely [here the "(+ Ol)" term indicates that the equilibrium exists in olivine-free portions of the system but with a higher variance]. This disappearance is probably accomplished by emergence from the system solidus of a critical end point to the Pgt + Aug (+ Ol) liquidus boundary curve at its low-temperature, Al-rich end followed by progressive elimination of the boundary curve as the critical end point migrates to the Opx-Wo join. The two-clinopyroxene curve, therefore, is analogous to the plagioclase + potassium feldspar boundary curve in the An-Ab-Or system (Stewart and Roseboom 1961; Nekvasil 1992), in which the anhydrous solidus progressively pulls out of the ternary feldspar solvus with increasing pressure and the critical end point to the two-feldspar curve migrates toward the Or-An join. Prior to the emergence of the critical end point to the Pgt + Aug (+ Ol) liquidus curve, the crest of the two-clinopyroxene solvus in a section with Mg′ and Al components appropriate to the local solidus liquid is metastable and at a higher temperature than the solidus liquid. The emergence of the critical end point implies that the temperature of the local solidus lies above a section of the aluminous portion of the ternary Pgt-Aug solvus and below the less aluminous remainder of the solvus. Initially, the critical end point emerges at a point analogous to either a or c in Figure 4, which thus becomes pseudoinvariant. At higher pressures the critical Cpx coexists only with Ol and liquid, and points analogous to a or c disappear.

A proposed set of topologies for the polybaric Ol liquidus surface is shown schematically in Figure 6. At 1 atm the critical end point to the Pgt + Aug (+ Ol) liquidus boundary curve is metastable with respect to Opx + liq in high Mg′ liquids (Fig. 6a) and metastable with respect to Pl + liq in intermediate Mg′ liquids (Fig. 6b). Thus, the polythermal fields of pyroxene composition are all separate. At some higher pressure (probably between 10 and 15 kbar), the critical end point becomes stable (Figs. 6c and 6d), portions of the Pgt and Aug composition fields that have expanded because of enhanced solubility of aluminous components become continuous, and the Cpx on the lherzolite solidus becomes supercritical. A section parallel to the Opx-Di join, but lying on the low-temperature side of the critical end point, would have phase relations analogous to the middle T-X section in Figure 3b; a section situated on the high-temperature side of the critical end point would have phase relations analogous to the lower T-X section in Figure 3b. Because of the proximity of the initial critical end point to the lherzolite-solidus liquid with intermediate Mg′ (Fig. 6d), the distortion of the clinopyroxene-solidus surface has a more pronounced effect on the composition of the intermediate-Mg′ clinopyroxene coexisting with orthopyroxene than on the high-Mg′ clinopyroxene (compare the martian and terrestrial panels in Fig. 5). Nonetheless, by 20 kbar the Pgt + Aug (+ Ol) liquidus curve must be completely eliminated, and the expansion of the compositional limits of the Cpx solid-solution field pushes the Opx + Cpx tieline to lower Wo along the Cpx field and hence lower CaO (Figs. 6e and 6f).

Some existing experimental data constrain this hypothesis. First, with respect to the intersection of the lherzolite solidus and the three-pyroxene equilibrium, no reports of the assemblage Ol + Pgt + Aug + Sp in liquids with Mg′ $\geq$ 0.60 in the range of 10–20 kbar are known to us. Because liquids with Mg′ $\geq$ 0.60 would be expected to have Ol + Opx + Aug + Pl as a possible assemblage at 1 atm, the Ol + Pgt + Aug + Sp assemblage would constitute a change from the topology in Figure 4a to that in Figure 4b with increasing pressure (also, Pl $\rightarrow$ Sp). Somewhat more difficult to distinguish are the assemblages Ol + Opx + Pgt (subcritical) + Sp and Ol + Opx + Cpx (supercritical) + Sp, in which Pgt and Cpx may have similar compositions. The former assemblage would also require the 4a $\rightarrow$ 4b topological change in liquids with Mg′ $\geq$ 0.60, whereas the latter would not. For example, Falloon and Green (1988, and unpublished data) reported Ol + Opx + Cpx + Sp + liq at 1360 °C and 15 kbar in which Cpx has 16 wt% CaO; but at 1380 °C and 18 kbar, Cpx in the same assemblage has only 11 wt% CaO. Given that there is >8 wt% Al_2O_3 in this latter Cpx and that Carlson and Lindsley (1988) calculated pressure of the Pgt + Di critical point in the Fe-free En-Di join to be 18 kbar, this

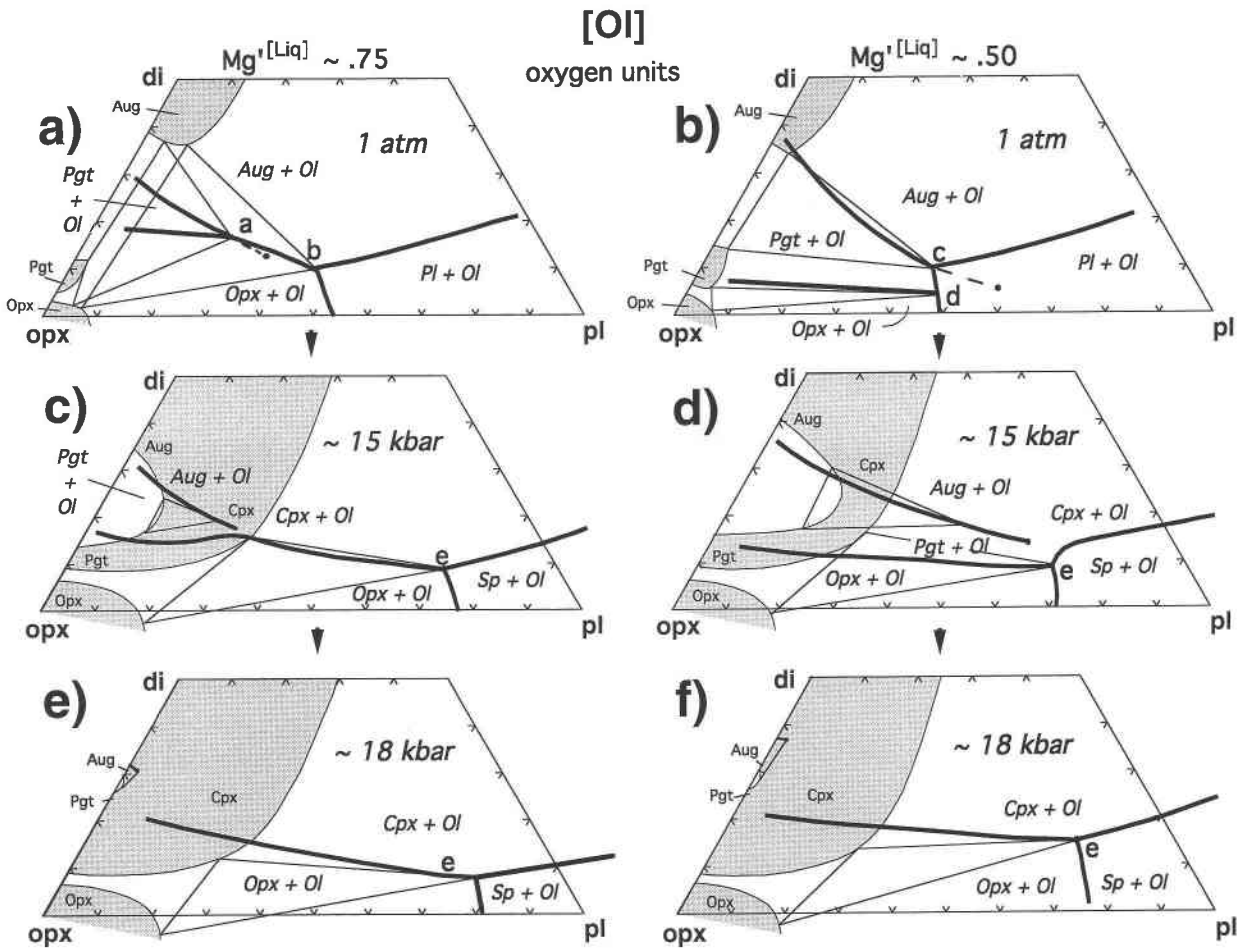

FIGURE 6. Schematic progression of liquidus boundaries and pyroxene solid-solution fields with pressure on the Ol saturation surface. Heavy curves are liquidus boundaries; light sold lines are tielines joining compositions of coexisting phases; shaded areas are polythermal fields of stable pyroxene composition. The letters a, b, c, and d refer to the same pseudounivariant equilibria shown in Figure 4; the letter e refers to pseudounivariant, lherzolitic solidus assemblages involving supercritical low-Ca clinopyroxene. The compositions of liquids with Mg′ = 0.75 and Mg′ = 0.50 are illustrated for the pressures 1 atm, 15 kbar, and 18 kbar in **a**, **c**, and **e**, and in **b**, **d**, and **f**, respectively.

low-Ca Cpx is likely, but not certain, to be supercritical. Second, although at least one example exists of the assemblage Ol + Opx + Pgt + Aug at 15 kbar [Takahashi and Kushiro (1983) reported this assemblage in a liquid with Mg′ = 0.64 (K21 #40)], and although the relatively high Al_2O_3 in this liquid (16.0 wt%) indicates that the Pgt + Ol + liq field has expanded with pressure, spinel is not present, so the three-pyroxene equilibrium has not reached the lherzolite solidus. Indeed, the data of Kinzler and Grove (1992) show liquids with similar Mg′ and saturated with the lherzolite assemblage as having Al_2O_3 concentrations of ~18 wt%.

The 15 kbar datum of Takahashi and Kushiro (1983) just discussed, plus others in their experiment table, indicate that the Pgt + Aug (+ Ol) liquidus boundary is still stable at this pressure. The presence of the liquidus boundary implies that the pressure interval between the first emergence of the critical end point and the elimination of the Pgt + Aug (+ Ol) liquidus boundary is no more than 2 or 3 kbar. Because the starting materials in the Takahashi and Kushiro (1983) experiments were mechanical mixtures and the phases present at the end of the experiments did not homogenize, some lingering doubts remain about the stability of the three-pyroxene assemblage. Nonetheless, Vander Auwera and Longhi (1994) reported the assemblage Opx + Pgt + Aug + Pl in ferroan liquids (Mg′ = 0.32) at 13 kbar. Although no change in topology, analogous to the change from Figure 4a to Figure 4b, is expected for these liquids because of the low Mg′ in the liquid, these data do support the stability of the three-pyroxene assemblage reported by Takahashi and Kushiro (1983) at 15 kbar. Together, these

two sets of data are consistent with those in the simple systems discussed above that show the Opx + Pgt + Aug + liq assemblage to be stable to approximately 15 kbar with little evidence of Mg′ dependence in the elimination of the Pgt + Aug two-phase field.

The implications of Cpx critical phenomena for modeling of planetary mantle melting are both considerable and complex. Although a critical end point to the Pgt + Aug + Ol liquidus curve apparently becomes stable at ~15 kbar and eliminates this curve by ~18 kbar over a wide range of composition, pronounced effects on Cpx composition occur at the lowest pressures during melting of spinel lherzolites with intermediate Mg′ because the critical end point emerges directly from the solidus. In such cases the solidus Cpx may be low in CaO (e.g., 9 wt%, Bertka and Holloway 1993) by 15 kbar. In CMAS and in the high Mg′ portion of the natural system, the critical end point emerges at a low-Al, spinel-absent point on the Ol liquidus surface where three pyroxenes—Opx, Pgt (subcritical low-Ca Cpx), and Aug (subcritical high-Ca Cpx)—are present. Thus, the Cpx critical phenomena do not directly affect melting of terrestrial spinel lherzolites. Nonetheless, the indirect effect is to produce Cpx with progressively lower CaO with increasing pressure as the solidus rolls over the inflected Cpx limb of the Opx + Cpx two-phase field (Fig. 1). Typically, CaO concentrations in solidus Cpx are in the range of 15–18 wt% near the spinel-plagioclase transition and decrease to ~10 wt% near the spinel-garnet transition (e.g., Falloon and Green 1988, and unpublished data; Kinzler 1996). The data of Kinzler (1996) also show that higher alkalies promote lower CaO in the solidus Cpx. By 28 kbar, however, the CaO concentration in Cpx along the garnet-lherzolite solidus is 5–8 wt% over a wide range of Mg′ and alkali concentration (Longhi 1995; Longhi and O'Connell 1996).

These considerations indicate not only that Cpx composition along the lherzolite solidus is a complex function of composition and pressure that needs to be accounted for in major element modeling, but also that there is much room for error in the use of partition coefficients (D) for trace elements. For example, recently Hauri et al. (1994) measured incompatible element partition coefficients at 25 kbar between Cpx with 17 wt% CaO and a basaltic liquid that is well removed from the lherzolite solidus where Cpx has about 8 wt% CaO (Longhi 1995). Applying the McKay et al. (1986) model for the composition dependence of REE partition coefficients to these different Cpx compositions leads to the prediction that the Hauri et al. (1994) coefficients would overestimate D_{La} by ~18× and D_{Lu} by ~1.3× if used to calculate lherzolite melting. Clearly, there is the potential for introducing both absolute and relative errors in geochemical calculations if variations in clinopyroxene composition are ignored.

Acknowledgments

We thank Rosamond Kinzler for sharing data with us and David Walker, Marie Johnson, and Rosamond Kinzler for their comments on an early version of this paper. We also thank Stearns A. Morse and Tibor Gasparik for their helpful reviews. This work was supported by grants from NASA (NAGW 3437; J.L., P.I.) and NSF (OCE-93-03028; V. Salters, P.I.) and by the Geophysical Laboratory of the Carnegie Institution of Washington and the Center for High Pressure Research. Lamont-Doherty Earth Observatory contribution no. 5455.

References cited

Bertka, C.M., and Holloway, J.R. (1993) Pigeonite at solidus temperature: Implications for partial melting. Journal of Geophysical Research, 98, 19755–19766.

——— (1994) Anhydrous partial melting of an iron-rich mantle: II. Primary compositions at 15 kbar. Contributions to Mineralogy and Petrology, 115, 323–338.

Boyd, F.R., and England, J.L. (1963) Effects of pressure on the melting of diopside, $CaMgSi_2O_6$, and albite, $NaAlSi_3O_8$, in the range up to 50 kilobars. Journal of Geophysical Research, 68, 311–323.

Carlson, W.D. (1988) Subsolidus phase equilibria on the forsterite-saturated join $Mg_2Si_2O_6$-$CaMgSi_2O_6$ at atmospheric pressure. American Mineralogist, 73, 232–241.

Carlson, W.D., and Lindsley, D.H. (1988) Thermochemistry of pyroxenes on the join $Mg_2Si_2O_6$-$CaMgSi_2O_6$. American Mineralogist, 73, 242–252.

Delano, J.W. (1977) Experimental melting relations of 63545, 76015, and 76055. Proceedings of the 8th Lunar Science Conference, 2097–2123.

Dreibus, G., and Wänke, H. (1985) Mars: A volatile rich planet. Meteoritics, 20, 367–382.

Falloon, T.J., and Green, D.H. (1988) Anhydrous partial melting of peridotite from 8 to 35 kbar and the petrogenesis of MORB. Journal of Petrology, Special Lithosphere Issue, 379–414.

Gasparik, T. (1990) A thermodynamic model for the enstatite-diopside join. American Mineralogist, 75, 1080–1091.

——— (1994) Mineral and chemical composition of the Earth's upper mantle. Eos, 75, 192–193.

Hauri, E.H., Wagner, T.P., and Grove, T.L. (1994) Experimental and natural partitioning of Th, U, Pb and other trace elements between garnet, clinopyroxene, and basaltic melts. Chemical Geology, 17, 149–166.

Herzberg, C., and Gasparik, T. (1991) Garnet and pyroxenes in the mantle: A test of the majorite fractionation hypothesis. Journal of Geophysical Research, 96, 16263–16274.

Huebner, J.S., and Turnock, A.C. (1980) The melting relations at 1 bar of pyroxenes composed largely of Ca-, Mg-, and Fe-bearing components. American Mineralogist, 65, 225–271.

Kinzler, R.J. (1996) Melting of mantle peridotite at pressures approaching the spinel to garnet transition: Application to the generation of mid-ocean ridge basalts. Journal of Geophysical Research, in press.

Kinzler, R.J., and Grove, T.L. (1992) Primary magmas of mid-ocean ridge basalts: 1. Experiments and methods. Journal of Geophysical Research, 97, 6907–6926.

Kushiro, I. (1969) The system forsterite-diopside-silica with and without water at high pressures. American Journal of Science, 276-A, 269–294.

Lindsley, D.H. (1980) Phase equilibria of pyroxenes at pressures > 1 atmosphere. In Mineralogical Society of America Reviews in Mineralogy, 7, 289–308.

——— (1981) The formation of pigeonite on the join hedenbergite-ferrosilite at 11.5 and 15 kbar: Experiments and a solution model. American Mineralogist, 66, 1175–1182.

——— (1983) Pyroxene thermometry. American Mineralogist, 68, 477–493.

Lindsley, D.H., and Dixon, S.A. (1976) Diopside-enstatite equilibria at 850 to 1400 °C, 5 to 35 kbars. American Journal of Science, 276, 1285–1301.

Lindsley, D.H., and Andersen, D.J. (1983) A two-pyroxene thermometer. Journal of Geophysical Research, 88, A887–A906.

Longhi, J. (1987) Liquidus equilibria and solid solution in the system $CaAl_2Si_2O_8$-Mg_2SiO_4-$CaSiO_3$-SiO_2 at low pressure. American Journal of Science, 287, 265–331.

——— (1991) Comparative liquidus equilibria of hypersthene-normative basalts at low pressure. American Mineralogist, 76, 785–800.

——— (1995) Liquidus equilibria of some primary lunar and terrestrial melts in the garnet stability field. Geochimica et Cosmochimica Acta, 59, 2375–2386.

Longhi, J., and Boudreau, A.E. (1980) The orthoenstatite liquidus field in the system forsterite-diopside-silica at one atmosphere. American Mineralogist, 65, 563–573.

Longhi, J., and Pan, V. (1988) A reconnaissance study of phase boundaries in low-alkali basaltic liquids. Journal of Petrology, 29, 115–148.

Longhi, J., and O'Connell, M.S. (1996) Experimental determination of low-degree melts of MORB mantle at 28 kbar. Eos, in press.

McKay, G.A., Wagstaff, J., and Yang, S.-R. (1986) Clinopyroxene REE distribution coefficients for shergottites: The REE content of the Shergotty melt. Geochimica et Cosmochimica Acta, 50, 927–937.

Nekvasil, H. (1992) Ternary feldspar crystallization in high-temperature felsic magma. American Mineralogist, 77, 592–604.

Sack, R.O., and Ghiorso, M. (1994) Thermodynamics of multicomponent pyroxenes: II. Phase relations in the quadrilateral. Contributions to Mineralogy and Petrology, 116, 287–300.

Schweitzer, E. (1982) The reaction pigeonite = diopside$_{ss}$ + enstatite$_{ss}$ at 15 kbar. American Mineralogist, 67, 54–58.

Stewart, D.B., and Roseboom, E.H., Jr. (1961) Lower temperature terminations of the three phase region plagioclase-alkali feldspar-liquid. Journal of Petrology, 3, 280–315.

Takahashi, E. (1986) Melting of a dry peridotite KLB-1 up to 14 GPa: Implications on the origin of peridotitic upper mantle. Journal of Geophysical Research, 91, 9367–9382.

Takahashi, E., and Kushiro, I. (1983) Melting of a dry peridotite at high pressures and basalt magma genesis. American Mineralogist, 68, 859–879.

Vander Auwera, J., and Longhi, J. (1994) Experimental study of a jotunite: Constraints on the parent magma composition and crystallization conditions, (P, T, f_{O_2}) of the Bjerkreim-Sokndal layered intrusion (Norway). Contributions to Mineralogy and Petrology, 118, 60–78.

Walter, M.J., and Presnall, D.C. (1994) Melting behavior of simplified lherzolite in the system CaO-MgO-Al_2O_3-SiO_2-Na_2O from 7 to 35 kbar. Journal of Petrology, 35, 329–359.

Manuscript received May 30, 1995
Manuscript accepted January 12, 1996